Predictive Current Control for Multilevel Cascaded H-Bridge Inverters Based on a Deadbeat Solution

Qi, Chen; Tu, Pengfei; Wang, Peng; Zagrodnik, Michael

2017

https://hdl.handle.net/10356/85213

https://doi.org/10.6113/JPE.2017.17.1.76

Predictive Current Control for Multilevel Cascaded H-Bridge Inverters Based on a Deadbeat Solution

Chen Qi[†], Pengfei Tu[*], Peng Wang[*], and Michael Zagrodnik[**]

[†,*]School of Electrical and Electronic Engineering, Nanyang Technological University, Jurong West, Singapore
[**]Advanced Technology Centre, Rolls-Royce Singapore Pte. Ltd., Jurong West, Singapore

Abstract

Finite-set predictive current control (FS-PCC) is advantageous for power converters due to its high dynamic performance and has received increasing interest in multilevel inverters. Among multilevel inverter topologies, the cascaded H-bridge (CHB) inverter is popular and mature in the industry. However, a main drawback of FS-PCC is its large computational burden, especially for the application of CHB inverters. In this paper, an FS-PCC method based on a deadbeat solution for three-phase zero-common-mode-voltage CHB inverters is proposed. In the proposed method, an inverse model of the load is utilized to calculate the reference voltage based on the reference current. In addition, a cost function is directly expressed in the terms of the voltage errors. An optimal control actuation is selected by minimizing the cost function. In the proposed method, only three instead of all of the control actuations are used for the calculations in one sampling period. This leads to a significant reduction in computations. The proposed method is tested on a three-phase 5-level CHB inverter. Simulation and experimental results show a very similar and comparable control performance from the proposed method compared with the traditional FS-PCC method which evaluates the cost function for all of the control actuations.

Key words: Computational burden, Deadbeat solution, Multilevel inverter, Predictive current control

I. INTRODUCTION

Multilevel inverters provide a cost-effective solution in medium-voltage high-power energy conversion [1]. Of the multilevel inverter topologies, the cascaded H-bridge (CHB) inverter is a popular and mature topology in the industry [2]. CHB inverters have been widely applied in three-phase reactive power compensation [3], renewable energy power generation [4], energy storage systems [5], and ac drives [6].

The current control of multilevel inverters with a fast dynamic response is always a challenge. The classic current control methods use linear control [7]. Applying linear control to a nonlinear converter can lead to uneven performance throughout the dynamic range [8]. New and advanced current control methods have been constantly evolving. Among them, the predictive current control (PCC) methods have received

increasing interest due to their outstanding capability in dynamics [9]. Deadbeat (DB) current control is one well-known PCC method providing a fast current tracking [10]. This DB solution utilizes an inverse model to calculate a desired voltage based on the current reference [10]. However, a modulator is required to apply the desired voltage and the modulation method is usually complex when it is implemented for multilevel inverters.

An alternative PCC method is the finite-set PCC (FS-PCC), which takes into account the discrete nature of power converters and a finite set of control actuations [11]-[18]. The advantages of this method include an intuitive concept, a fast dynamic response, and the lack of a modulator [11]. The FS-PCC method solves a rolling optimization problem where a discrete model is established to predict future currents and a cost function related to the current errors is evaluated for each possible actuation. Optimal actuation to minimize the cost function is applied in the next sampling period [12], [13]. However, a main drawback of the FS-PCC is its large computational burden [15]. For the application of CHB inverters which have a large number of switching states and redundancies, the computational burden increases

exponentially. This in turn, requires a reduced sampling frequency compared with other control methods [15]-[18]. In CHB inverters, reductions of the control complexity and computational burden have become important issues for the successful implementation of the FS-PCC method. Some efforts have been reported in [19]-[21]. These methods choose a subset of control actuations. However, they degrade the dynamic response since only an adjacent voltage level of a CHB inverter is available in next sampling period even if a big change is desired [19]-[21].

In this paper, a FS-PCC method based on a DB solution to reduce the computational burden is proposed for three-phase zero-common-mode-voltage (ZCMV) CHB inverters (see Fig. 1(a)). With the DB solution, only the voltage levels near the reference voltage are expected control actuation (ZCMV voltage level combination (VLC)). To select this control actuation from these voltage levels, a cost function of the absolute error between the reference voltage and the voltage level is defined, and a simple procedure for selecting the control actuation is developed in the proposed FS-PCC (PFS-PCC) method. By means of the PFS-PCC method, only three control actuations are necessary to evaluate the cost function and the one minimizing the cost function is selected, leading to a considerable reduction in computations compared with the traditional FS-PCC (TFS-PCC) method where all of the control actuations are used to evaluate the cost function, which is defined as the current error. Nevertheless, the steady-state and dynamic performances, which are comparable to those of the TFS-PCC method, are achieved by the proposed method due to the DB solution.

This paper is organized as follows. In Section II, descriptions of the ZCMV CHB inverter and the computational burden of the TFS-PCC method are presented. In Section III, discrete inverse models of the RL load and permanent magnet synchronize motor (PMSM) are derived. In Section IV, the proposed method is presented. Simulation analysis and experimental results for comparing proposed method with the TFS-PCC are presented in section V and VI, respectively. Finally, some conclusions are presented in section VII.

II. ZCMV CHB INVERTER AND THE COMPUTATIONAL BURDEN OF THE TFS-PCC METHOD

A. ZCMV CHB Inverter

As shown in Fig. 1(a), N H-bridge cells are connected in series on their ac sides. Each cell is powered by a dc supply of voltage E, and can produce three output voltages $-E$, 0, and E. The leg voltage of the CHB inverter is the summation of the output voltages of the cells. Therefore, the maximum number of voltage levels in each leg is $2N+1$.

When the three-phase loads are connected to a neutral, the output voltage across the load is obtained by subtracting the common-mode voltage (CMV) v_{cm} from the leg voltage. The
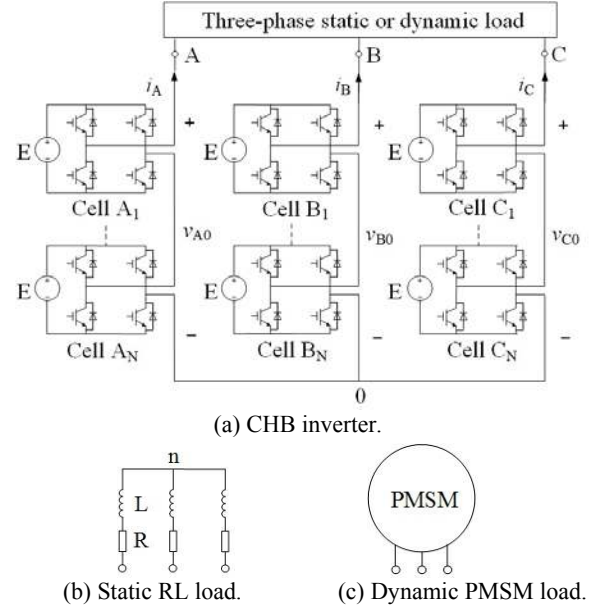

(a) CHB inverter.

(b) Static RL load.   (c) Dynamic PMSM load.
Fig. 1. Three-phase $(2N+1)$-level CHB inverter.

CMV induced by the sum of the three-phase leg voltages v_{A0}, v_{B0}, and v_{C0} is given by:

$$v_{cm} = \frac{v_{A0} + v_{B0} + v_{C0}}{3} \tag{1}$$

The CMV may result in motor bearing damage, electromagnetic interference problems and zero-sequence relay false trips [22]. Fortunately, it is possible for multilevel inverters with odd levels to eliminate CMV due to existence of some special combinations of three-phase voltage levels which generate zero v_{cm}. To achieve this, only those ZCMV VLCs which are considered as control actuations are used to evaluate the cost function in this paper. By applying zero v_{cm}, the leg voltage reference is always equal to the desired output voltage which can be obtained on the basis of the DB solution.

The CHB inverter can connect to either static or dynamic loads. RL loads and PMSMs are widely-used static and dynamic loads, as shown in Fig. 1(b) and (c). Many illustrations of the TFS-PCC and DB control methods for driving these two loads have been presented in [10], [11], [19], and [23]-[25]. In proposed method based on a DB solution, reference voltages are necessary but the modulator is avoided. The proposed method selects the optimal control actuation on the load by minimizing the cost function. However, unlike the TFS-PCC, the proposed method based on a DB solution needs to evaluate the cost function for only three instead of all of the control actuations, avoiding exhaustive searches and reducing the computations. Therefore, the proposed method can be seen as a special case of the FS-PCC method.

B. Computational Burden of the TFS-PCC Method

When N cells are connected in cascade for CHB inverters, there is a total of $(2N+1)^3$ VLCs. However, some of them are redundant. In ZCMV CHB inverters, the VLCs are non-redundant and their amount is reduced to $3N^2+3N+1$.

Cell number in each leg	Level number	Total VLC number	ZCMV VLC number
1	3	27	7
2	5	125	19
•••	•••	•••	•••
6	13	2197	127
N	$2N+1$	$(2N+1)^3$	$3N^2+3N+1$

Still, the number of ZCMV VLCs rises exponentially and becomes extremely high when the cell number N is large. An illustration of relationship between the cell number and the VLC number is shown in Table I. It can be noted from Table I, for example, that when 6 cells are employed, 127 ZCMV VLCs are candidates for evaluating the cost function in the TFS-PCC method, which cause a considerable computational burden. This computational burden is unacceptable even if a fast DSP or an FPGA is adopted. The proposed method is focused on solving this issue. A significant reduction in the computations is achieved in the proposed method since only three candidates are necessary for any number of cells.

On the other hand, the same voltage level has redundant switching states. The total number of switching states is 4^{3N}. The elimination of redundant switching states does not affect the behavior of the current control, because the possible voltage levels applied on the load does not change [19]. For comparing the control performance of the TFS-PCC and the proposed method, the redundancy of CHB inverters is not utilized in this paper.

III. INVERSE MODELS OF STATIC AND DYNAMIC LOADS

The proposed method is based on a DB solution to reduce the control actuations. As previously mentioned, the DB solution for the PFS-PCC is to utilize an inverse load model to calculate the desired voltage based on the current reference. The RL load and PMSM representing the static and dynamic loads are studied in this paper, and their inverse models are given as follows.

A. RL Load Inverse Model

For the ZCMV, the output current of phase A through the resistance R and the inductance L at the $k+1$ instant can be represented in the discrete-time domain as:

$$i_A(k+1) = \frac{T_s}{L}v_{A0}(k) - \frac{RT_s - L}{L}i_A(k) \qquad (2)$$

where T_s is a sampling period.

Assuming that the one-step-forward output current becomes equal to the one-step-forward reference current by applying the reference voltage, the output currents in (2) can be expressed by the inverse model as [23]:

$$v_{A0}^*(k) = \frac{L}{T_s}i_A^*(k+1) + \frac{RT_s - L}{T_s}i_A(k) \qquad (3)$$

In the inverse model given in (3), the reference current is expressed directly in terms of the reference voltage. Since only the voltage levels near the reference voltages can be the expected output, an exhaustive search for the optimal voltage level in the TFS-PCC is avoided by using this inverse model.

In real implementations, there is a one-step delay caused by the update mechanism in modern digital controllers. To compensate for the influence caused by the one-step delay, shift the inverse model in (3) by one-step forward. Then the reference voltage at the $k+1$ instant is used as:

$$v_{A0}^*(k+1) = \frac{L}{T_s}i_A^*(k+2) + \frac{RT_s - L}{T_s}i_A(k+1) \qquad (4)$$

In (4), the reference current at the $k+2$ instant can be calculated from the Lagrange extrapolation using the present and the past two reference values as [23]:

$$i_A^*(k+2) = 3i_A^*(k+1) - 3i_A^*(k) + i_A^*(k-1) \qquad (5)$$

Similar equations for phases B and C can be derived from (2)-(5).

B. PMSM Inverse Model

In the dq reference frame, the PMSM can be modeled in the discrete-time domain as [19]:

$$\begin{bmatrix} i_d(k+1) \\ i_q(k+1) \end{bmatrix} = A\begin{bmatrix} i_d(k) \\ i_q(k) \end{bmatrix} + B\begin{bmatrix} v_d(k) \\ v_q(k) \end{bmatrix} + C \qquad (6)$$

where:

$$A = \begin{bmatrix} 1 - R_sT_s/L_d & L_qT_s\omega_e(k)/L_d \\ -L_dT_s\omega_e(k)/L_q & 1 - R_sT_s/L_q \end{bmatrix} \qquad (7a)$$

$$B = \begin{bmatrix} T_s/L_d & 0 \\ 0 & T_s/L_q \end{bmatrix} \qquad (7b)$$

$$C = \begin{bmatrix} 0 \\ -\psi_{PM}T_s\omega_e(k)/L_q \end{bmatrix} \qquad (7c)$$

In (6) and (7), i_d and i_q along with v_d and v_q are the d- and q-axis stator currents and voltages, R_s is the stator resistance, L_d and L_q are the d- and q-axis stator inductances, ω_e is the rotor electrical angular velocity, and ψ_{PM} is the flux linkage established by the permanent magnets of the rotor. Similar to RL loads and with the same compensation mechanism, assuming that the d- and q-axis currents are equal to the d- and q-axis reference currents at the $k+2$ instant by applying the d- and q-axis reference voltages at the $k+1$ instant, the inverse model of the PMSM can be expressed as:

$$\begin{bmatrix} v_d^*(k+1) \\ v_q^*(k+1) \end{bmatrix} = E\begin{bmatrix} i_d^*(k+2) \\ i_q^*(k+2) \end{bmatrix} + F\begin{bmatrix} i_d(k+1) \\ i_q(k+1) \end{bmatrix} + G \qquad (8)$$

where:

$$E = \begin{bmatrix} L_d/T_s \\ L_q/T_s \end{bmatrix} \qquad (9a)$$

$$F = \begin{bmatrix} R_s - L_d/T_s & -L_q\omega_e(k+1) \\ L_d\omega_e(k+1) & R_s - L_q/T_s \end{bmatrix} \qquad (9b)$$

$$G = \begin{bmatrix} 0 \\ \psi_{PM} \omega_e(k+1) \end{bmatrix} \quad (9c)$$

For a sufficiently small sampling period, the method considers $\omega_e(k+1) \approx \omega_e(k)$.

IV. PROPOSED METHOD

A. Cost Function of the TFS-PCC

For tracking the reference current, the TFS-PPC method directly presents this objective in a cost function. The following two cost functions $g_{TFS-PCC}^{RL}$ [13] and $g_{TFS-PCC}^{PMSM}$ [25] for the RL load and PMSM are widely used in the TFS-PCC and are given by:

$$g_{TFS-PCC}^{RL} = \left| i_A^*(k+2) - i_A(k+2) \right| + \left| i_B^*(k+2) - i_B(k+2) \right|$$
$$+ \left| i_C^*(k+2) - i_C(k+2) \right| \quad (10)$$

$$g_{TFS-PCC}^{PMSM} = \left| i_d^*(k+2) - i_d(k+2) \right| + \left| i_q^*(k+2) - i_q(k+2) \right| \quad (11)$$

In (10), $i_A(k+2)$, $i_B(k+2)$, and $i_C(k+2)$ are the predicted output currents of CHB inverters by shifting (2) one-step forward. Similarly, the predicted d- and q-axis stator currents $i_d(k+2)$ and $i_q(k+2)$ are obtained by shifting (6) one-step forward. By controlling the d-axis oriented to the rotor magnetic field and the q-axis oriented to the stator current vector, the d-axis stator current becomes zero and the q-axis stator current is proportional to the electrical torque. In this way, the machine control is implemented as a current control scheme [25]. Therefore, the PCC scheme can be effective for the PMSM control, where the d- and q-axis stator currents are expected to be zero and reference value, respectively. Thus, in (11), $i_d^*(k+2)$ is set to zero and $i_q^*(k+2)$ can be generated by the external speed control loop.

B. Cost Function of PFS-PCC

As previously mentioned, the DB solution is to utilize an inverse model to calculate the reference voltage based on the reference current. The proposed method is based on the DB solution and tracks the reference voltage instead of the reference current. Therefore, the cost functions for the RL load and PMSM in the proposed method are given by:

$$g_{PFS-PCC}^{RL}(k+1) = \left| v_{A0}^*(k+1) - v_{A0}(k+1) \right|$$
$$+ \left| v_{B0}^*(k+1) - v_{B0}(k+1) \right| + \left| v_{C0}^*(k+1) - v_{C0}(k+1) \right| \quad (12)$$

$$g_{PFS-PCC}^{PMSM}(k+1) = \frac{1}{L_d} \left| v_d^*(k+1) - v_d(k+1) \right|$$
$$+ \frac{1}{L_q} \left| v_q^*(k+1) - v_q(k+1) \right| \quad (13)$$

The reference voltages in (12) and (13) can be calculated by using inverse models which are given in (4) and (8) for the RL load and PMSM, respectively. In turn, the reference currents at the $k+2$ instant can be expressed from the inverse
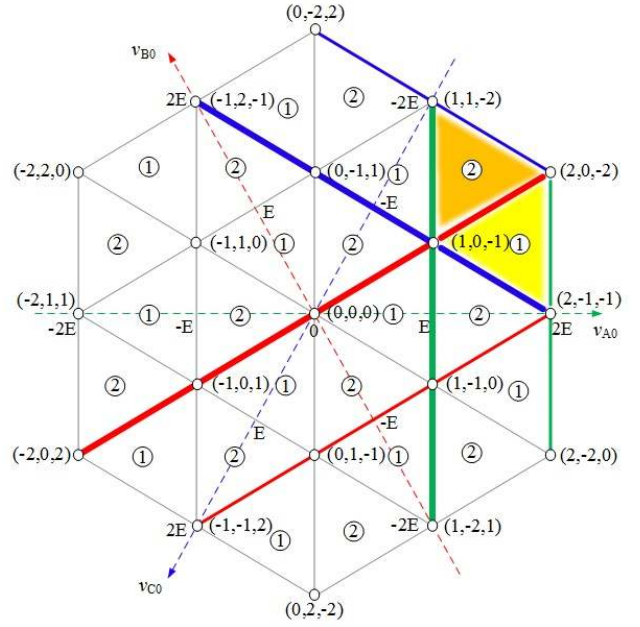

Fig. 2. All of the ZCMV VLCs for a three-phase 5-level CHB inverter.

models. By substituting these reference currents and predicted currents at the $k+2$ instant into (10) and (11), the cost functions of the TFS-PCC can be represented by (12) and (13) as:

$$g_{TFS-PCC}^{RL} = \frac{T_s}{L} g_{PFS-PCC}^{RL} \quad (14)$$

$$g_{TFS-PCC}^{PMSM} = T_s g_{PFS-PCC}^{PMSM} \quad (15)$$

It should be noted from (14) and (15) that the control actuation which minimizes the cost function of the PFS-PCC leads to the minimum cost function of the TFS-PCC. However, the cost function of the PFS-PCC is directly expressed in terms of the voltage signals which are more intuitive for selecting the control actuation compared with the current signals. For the minimum cost function, only the voltage levels near the reference voltage can be candidates. In CHB inverters, each leg has two adjacent voltage levels. One is higher than the reference voltage and the other is lower. Three legs can generate 8 VLCs. However, only three of them are ZCMV VLCs. Consequently, a big reduction in the computational burden is achieved with the DB solution.

C. Three ZCMV VLCs

The three ZCMV VLCs can be obtained according to Fig. 2, where all of the possible ZCMV VLCs for a 5-level CHB inverter are illustrated and represented by small cycles. Each cycle is the intersection of the three lines corresponding to the three leg voltages of phase A, B, and C, respectively. The VLC (v_{A0}, v_{B0}, v_{C0}) is marked by three corresponding numbers. For example, the numbers for (v_{A0}, v_{B0}, v_{C0}) = (E, 0, -E) is (1, 0, -1).

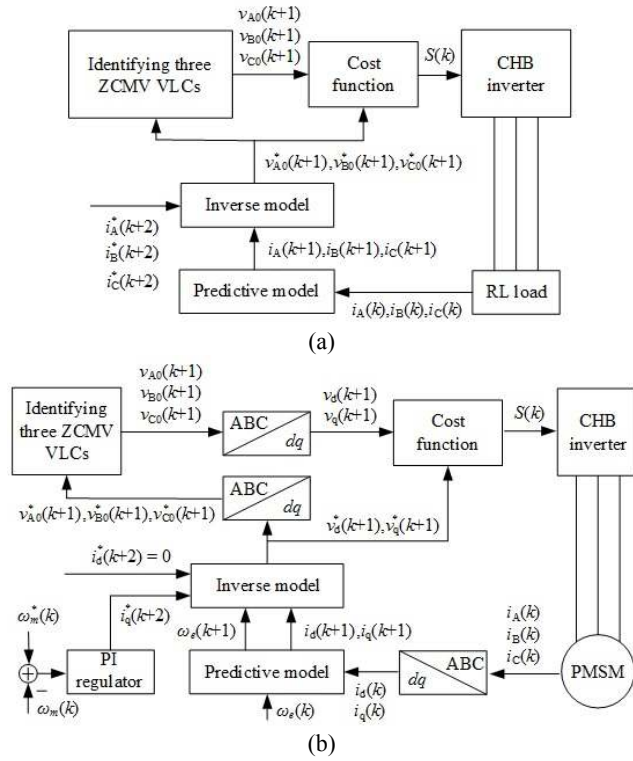In Fig. 2, a triangle with three cycles on its vertexes is

Fig. 3. Block diagram of the PFS-PCC method for (a) RL load and (b) PMSM.

located by six lines, two of which correspond to the two adjacent voltage levels of each leg. The upper and lower voltage levels for phase A, B and C are represented by v_{AU}, v_{BU}, and v_{CU} along with v_{AL}, v_{BL}, and v_{CL}, respectively. Obviously, the three ZCMV VLCs must belong to one of these triangles. The triangle can be identified by the sum of the three upper levels v_{AU}, v_{BU}, and v_{CU}. If the sum is E, the triangle is ①. Otherwise, the triangle is ②. In triangle ①, the ZCMV VLCs are (v_{AL}, v_{BU}, v_{CU}), (v_{AU}, v_{BL}, v_{CU}), and (v_{AU}, v_{BU}, v_{CL}) and in triangle ②, they are (v_{AU}, v_{BL}, v_{CL}), (v_{AL}, v_{BU}, v_{CL}), and (v_{AL}, v_{BL}, v_{CU}).

D. Implementation of the PFS-PCC

The basic idea of the PFS-PCC based on a DB solution is that the inverse model is used to calculate the reference voltage based on the reference current. As a result, the optimization process is reduced. Block diagrams of the PFS-PCC for the RL load and PMSM are shown in Fig. 3, where the main difference between the controls of the RL load and PMSM is that the PMSM control needs to be implemented in the *dq* reference frame.

A flow diagram of the PFS-PCC is described in Fig. 4. For the RL load, the steps for calculating $i(k+1)$, $i^*(k+2)$, $v^*(k+1)$, and $g_j(k+1)$ in Fig. 4 are executed in the *ABC* reference frame. However, they are transformed to the *dq* reference frame for the PMSM. It can be noted from Fig. 4 that the proposed method based on a DB solution evaluates the cost function for only three control actuations. A considerable reduction in
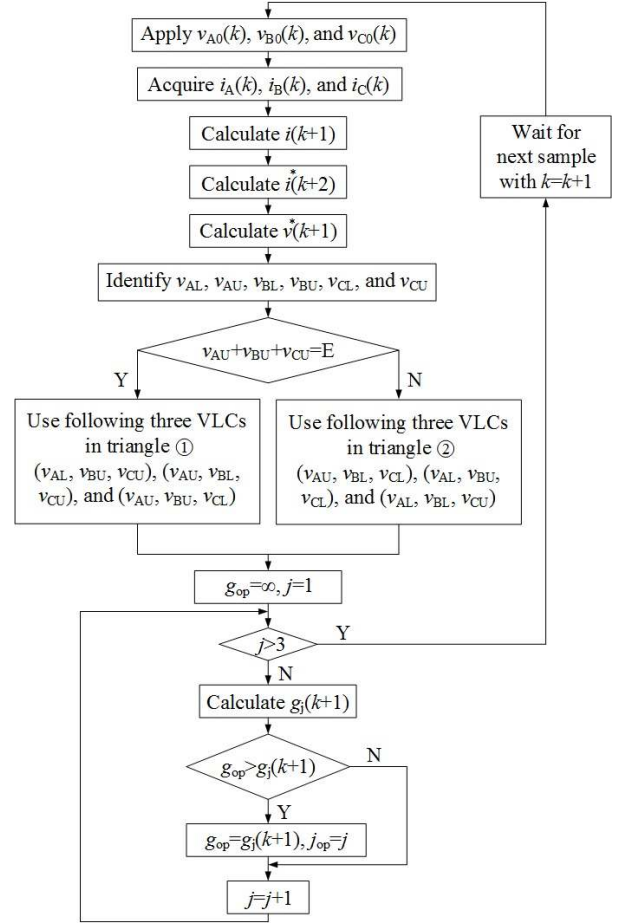

Fig. 4. Flow diagram of PFS-PCC method.

the computational burden is achieved in the PFS-PCC compared with the TFS-PCC method which has an exhaustive search process for all of the control actuations.

E. Proposed Method for Non-ZCMV CHB Inverters

For non-ZCMV CHB inverters, the reference voltages in (12) and (13) cannot be obtained directly from the inverse model of the load because the leg voltage is unequal to the output voltage across the load. The leg voltage is a summation of the output voltage and v_{cm} which is given in (1). In turn, v_{cm} is induced by the sum of the three-phase leg voltages v_{A0}, v_{B0}, and v_{C0}. As a result, the number of control actuations (v_{A0}, v_{B0}, v_{C0}), which is used to evaluate the cost function, must exceed three. The proposed method loses its significant reduction in the computational burden for the application of non-ZCMV CHB inverters.

V. SIMULATION ANALYSIS

Simulation models of the control systems for the RL load and PMSM connected to a 5-level CHB inverter are examined in the PLECS environment. To offer an impartial and valuable reference, all of the simulation results are shown under the same conditions. The simulation conditions are
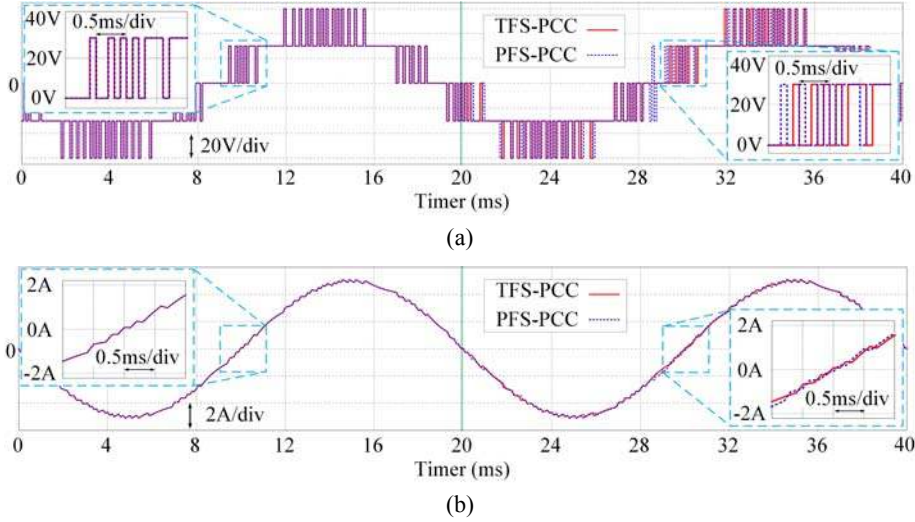
(a)

(b)

Fig. 5. Simulated waveforms of (a) leg voltages and (b) output currents of TFS-PCC and PFS-PCC methods for a single-phase 5-level CHB inverter.

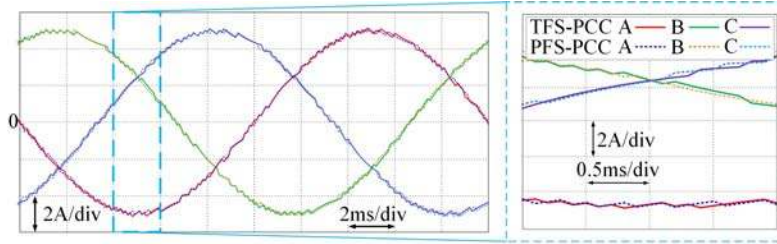Fig. 6. Simulated waveforms of output currents of TFS-PCC and PFS-PCC methods for a three-phase 5-level ZCMV CHB inverter.

listed in Table II.

A. Current Control Behaviors of the RL Load with the TFS-PCC and the PFS-PCC

Although the same reference current can be used in TFS-PCC and PFS-PCC, the current control behavior may not be identical. This is because the next behavior of the control variables in the FS-PCC is affected by last one, which is measured at the beginning of sampling period. The simulated waveforms of the leg voltages and output currents of the TFS-PCC and PFS-PCC methods are illustrated in Fig. 5, where a single-phase 5-level CHB inverter is controlled. In the simulation, a random noise varying between -0.05 and 0.05 (1% reference current) is added to the measured current of the PFS-PCC method after a time of 20ms. It can be noted from Fig. 5 that the TFS-PCC and PFS-PCC methods have completely coincident voltages as well as current waveforms before the time of 20ms. During that time, the measured currents of the TFS-PCC and PFS-PCC methods in each corresponding sampling period are identical. However, after a random noise added, a difference in the waveforms appears.

Unlike single-phase inverters, three-phase inverters have three current control targets which need to be achieved in a single cost function. Therefore, it is more difficult for the TFS-PCC and PFS-PCC methods to have a completely coincident waveform. Fig. 6 shows simulated waveforms of

TABLE II
SIMULATION PARAMETERS

E	30V	Pole pairs	4
T_s	100μs	Inertia	3.1×10^{-5} kgm^2
R/L	8Ω /10mH	Dead Time	2μs
R_s	4.7Ω	PI regulator output limit	-1.2/1.2
L_d/L_q	7.05/3.85mH	K_p	0.1
ψ_{PM}	0.1068Wb	K_i	1

the output currents of the TFS-PCC and PFS-PCC methods for a three-phase 5-level ZCMV CHB inverter, where no noise is added to the measured currents. Nevertheless, some differences in the waveforms appear in each phase.

Further evaluations of the steady-state and dynamic performances in the control of the RL load are shown in the experimental results.

B. Control Behaviors of the PMSM with the TFS-PCC and PFS-PCC Methods

The validity of the PMSM drive with the proposed method has been investigated in simulations. A comparison of the results of the control behavior of the PMSM with the TFS-PCC and PFS-PCC methods is shown in Fig. 7, where n is the rotor speed, T_m is the load torque, and T_e is the electrical torque. It can be noted from Fig. 7 that the
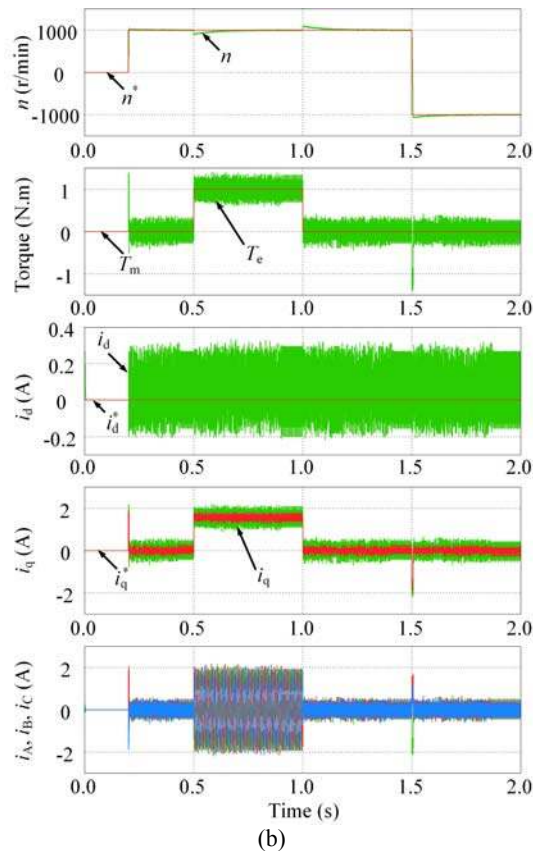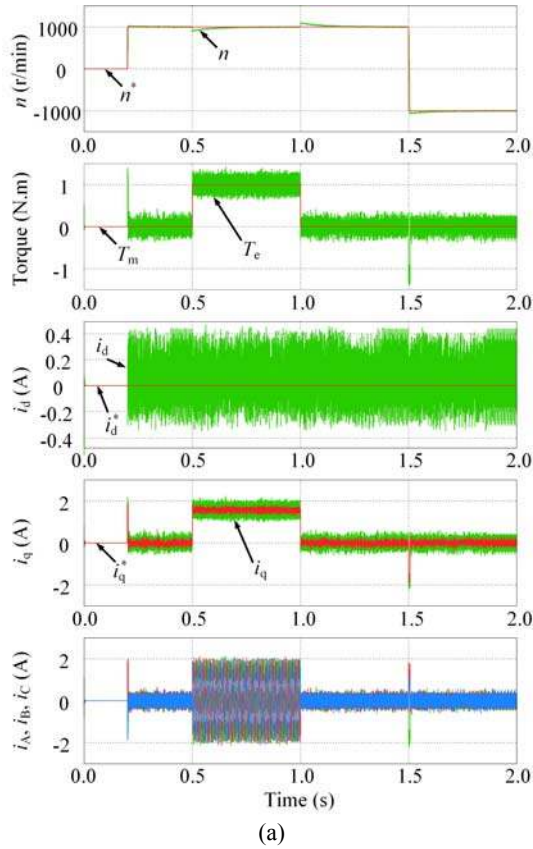
(a)

(b)

Fig. 7. Simulated responses of PMSM drive with (a) TFS-PCC and (b) PFS-PCC methods to step changes of the reference velocity and load torque.
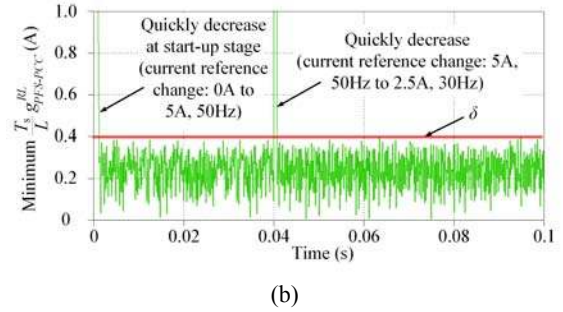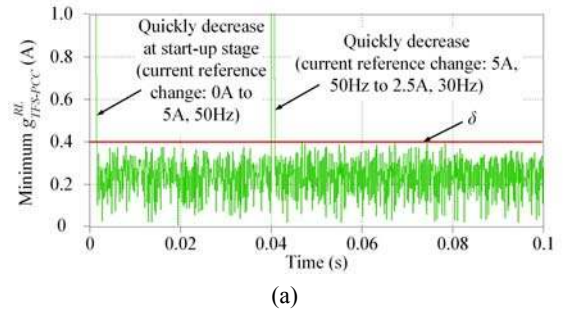

(a)

(b)

Fig. 8. Convergence of the minimum cost function bounded by δ for (a) TFS-PCC and (b) PFS-PCC methods with RL load under large current reference step changes.

TFS-PCC and PFS-PCC methods have very similar responses in the PMSM drive even though they adopt different cost functions and have a big difference in their computational burdens. The q-axis stator current is properly limited to 2A during startup. When the load torque is imposed from 0.5s to 1.0s, the value of the q-axis current increases quickly to its reference value. The q-axis current limitation (i_q=-2A) can also be observed in the speed reversal. The zero d-axis stator current is also realized in the TFS-PCC and PFS-PCC methods.

C. Practical Stability of the System

As depicted in [26] and [27], the practical stability of the system is guaranteed when the system state $x(k)$ is bounded at around the desired system reference x^*. The practical term is used to emphasize that only the stability in the neighborhood of the system reference can be established [26]. In essence, the controller is designed to ensure that the tracking error $x(k)-x^*$ (the absolute value is normally used to define the cost function) decays over time until finally reaching the neighborhood of the reference. See [26] and [27] for a more thorough presentation. From this intuitive idea, the evidence that the closed-loop systems for TFS-PCC and PFS-PCC laws have practical stability with a large reference step change is given in Fig. 8, where the vertical axis is the minimum value from all of the possible cost functions. The control actuation, which leads to this minimum cost function, is selected in the FS-PCC method. Similar trajectories along with the current reference changes for the TFS-PCC and PFS-PCC methods can be seen from Fig. 8, where the value of the minimum cost functions monotonically decrease until they are bounded by a
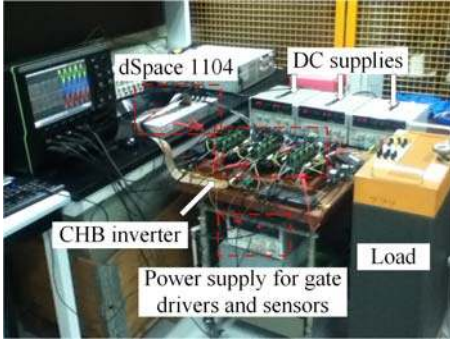
(a) Overview of experimental platform.
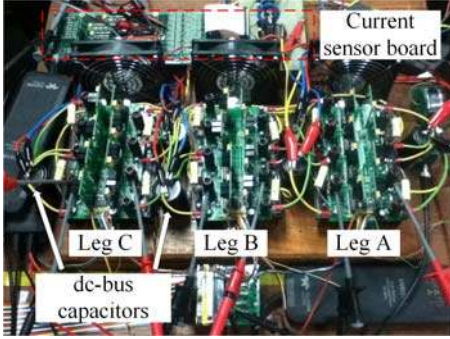
(b) Detailed view of CHB inverter.

Fig. 9. Experimental platform of a three-phase 5-level CHB inverter.

desired value δ. The value of δ can be used to characterize the closed-loop performance of the system in terms of the steady-state error, which cannot reach zero due to the switching action occurring at discrete instants [27].

VI. EXPERIMENTAL RESULTS

In order to verify the control performance of the proposed method, some experiments for the RL load were carried out in the laboratory. Fig. 9 shows the experimental platform of the three-phase 5-level CHB inverter. The proposed control method along with the TFS-PCC method are implemented on a dSPACE DS1104 controller board and the two H-bridge cells of the CHB inverter are powered by a regulated dc voltage supply with two isolated output voltages.

The conditions of the experiment are same as those of the simulation. The experimental waveforms shown in the following are carried out at a sampling frequency of 10kHz. Further comparisons between the TFS-PCC and PFS-PCC methods with different sampling frequencies were also provided.

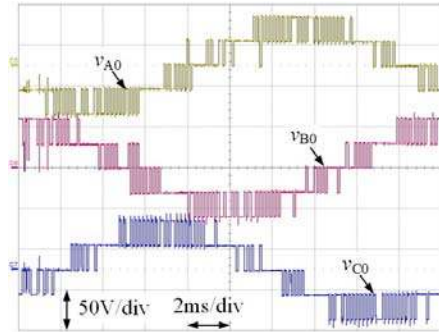### A. Steady-state and Dynamic Performances

Fig. 10 shows experimental waveforms of the output currents and voltages of the TFS-PCC and PFS-PCC methods for a three-phase 5-level ZCMV CHB inverter, where the amplitude I_{rm} and frequency f_r of the reference current are 5A and 50Hz, respectively. It can be seen in Fig. 10 that both
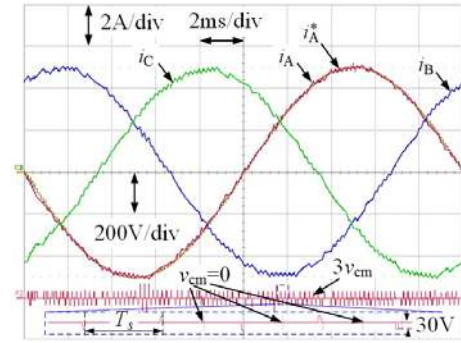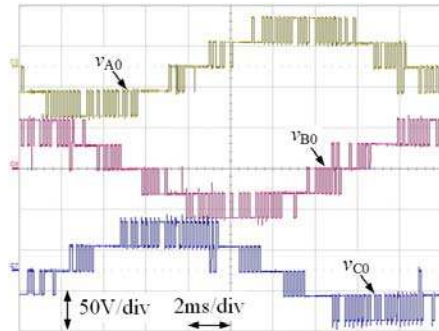

(a)
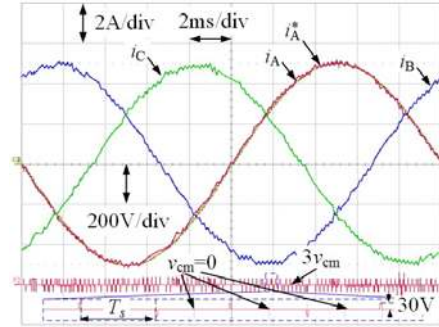
(b)

(c)

(d)

Fig. 10. Experimental waveforms of (a) and (b) output currents and $3v_{cm}$ and (c) and (d) leg voltages at steady state with current reference of 5A and 50Hz. (TFS-PCC method: (a) and (c); PFS-PCC method: (b) and (d)).

methods have very good reference tracking and different voltage waveforms. The $3v_{cm}$ of the CHB inverter and the details for the TFS-PCC and PFS-PCC methods are shown at the bottom of Fig. 10 (a) and (b), where the waveform of the
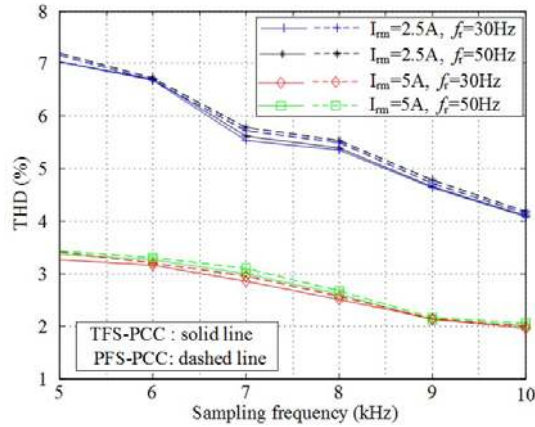
Fig. 11. THD of output currents of TFS-PCC and PFS-PCC methods with different sampling frequencies and current references.
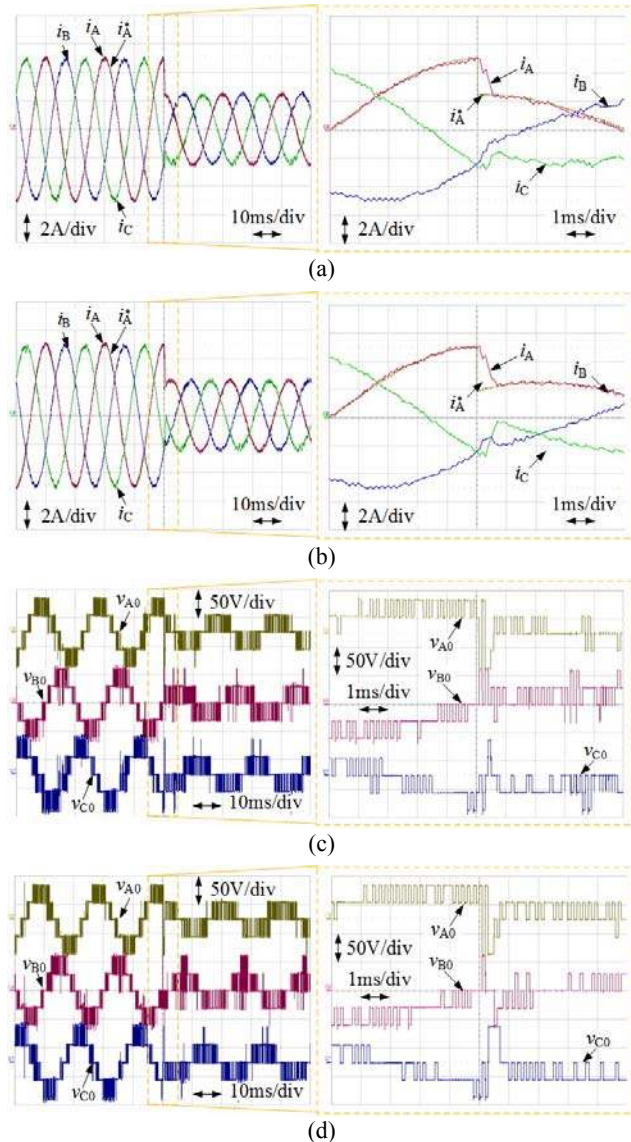

(a)

(b)

(c)

(d)

Fig. 12. Experimental waveforms of (a) and (b) output currents and (c) and (d) output voltages at dynamics with a step change of current reference from 5A into 2.5A. (TFS-PCC method: (a) and (c); PFS-PCC method: (b) and (d)).
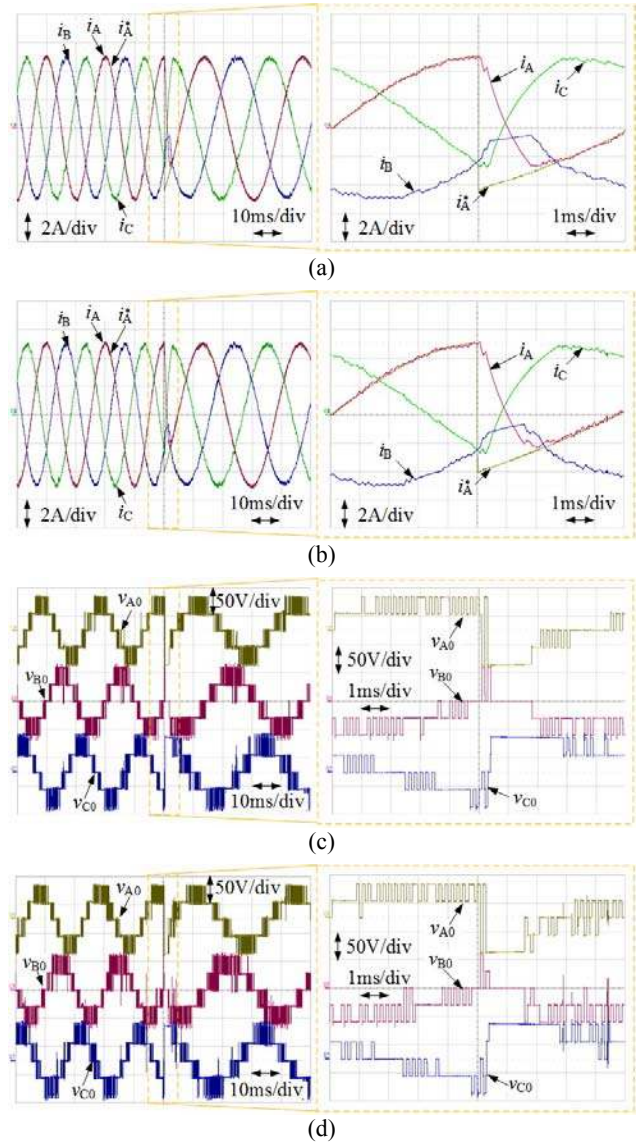

(a)

(b)

(c)

(d)

Fig. 13. Experimental waveforms of (a) and (b) output currents and (c) and (d) output voltages at dynamics with a step change of current reference from 50Hz into 30Hz. (TFS-PCC method: (a) and (c); PFS-PCC method: (b) and (d))

voltage $3v_{cm}$, which is equal to $v_{A0}+v_{B0}+v_{C0}$, is obtained by using the sum function in the oscilloscope. As shown in the detailed view of $3v_{cm}$, a zero CMV is obtained in each sampling period. However, a pulse whose width has a dead time of 2μs and a height of 30 V (dc supply voltage E) unavoidably exists during the commutation process.

Further comparisons of the output currents of the TFS-PCC and PFS-PCC methods are shown in Fig. 11, where the THDs of output currents with different sampling frequencies and references are calculated using the experimental data. The TFS-PCC and PFS-PCC methods have very similar and comparable THDs. The smaller reference leads to a somewhat larger THD of the current because the output levels are reduced and different reference frequencies have little effects on the THD. It can be observed in Fig. 11 that a
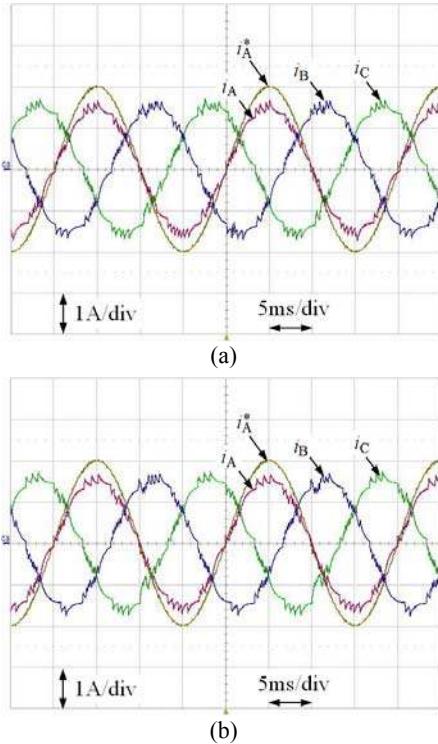
(a)

(b)

Fig. 14. Experimental waveforms of output currents of (a) TFS-PCC and (b) PFS-PCC methods when the R is three times the nominal value.
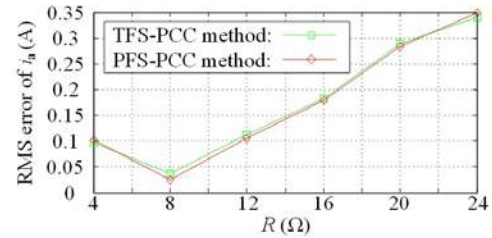

Fig. 15. RMS error of output current for variations of load resistance value.

provide similar steady-state current waveforms.

The performances of the TFS-PCC and the PFS-PCC methods are evaluated by calculating the RMS error of the output currents for variations of the load resistance value, as shown in Fig. 15. In Fig. 15, it can be seen that both methods have similar RMS current errors. This error value increases with a larger difference between the real and nominal load resistance values.

VII. CONCLUSIONS

An FS-PCC method based on a DB solution for ZCMV CHB inverters is proposed in this paper. In the proposed method, a cost function is directly expressed in terms of the control actuation and only three control actuations are used to evaluate the cost function with the help of the DB solution. The computational burden is significantly reduced in the proposed method compared with the TFS-PCC method, which evaluates the cost function for all of the control actuations. Finally, the very similar and comparable control performances of the proposed method and the TFS-PCC method are verified by simulation and experimental results. The proposed method can be an attractive alternative in CHB inverter applications where low computations are required.

ACKNOWLEDGMENT

decreasing THD is obtained as the sampling frequency increases. However, this results in a shorter time for executing the control algorithm in the digital controller.

A comparison of the dynamic performances of the PFS-PCC method with those of the TFS-PCC method is presented in Fig. 12 and 13, where step changes of the reference amplitude and frequency are applied. As shown in Fig. 12-13 (c) and (d), an extreme voltage change is generated to quickly track the reference in both the TFS-PCC and PFS-PCC methods. In these two methods, a very similar dynamic current is obtained, as shown in the detailed view of Fig. 12-13 (a) and (b), but with different voltage waveforms in the detailed view of Fig. 12-13 (c) and (d).

B. Parameter Variation

The current behavior of the CHB inverter under variations of its parameters is evaluated in experimental tests, where the load resistance R is varied and the load inductance L is kept at its nominal value. The varying range of R is 4Ω to 24Ω. As shown in Table II, the nominal values of R and L are 8Ω and 10mH, respectively.

Fig. 14 shows experimental waveforms of the output currents of the TFS-PCC and PFS-PCC methods at the steady state, where the load resistance R is three times the nominal value. In Fig. 14, large steady-state current error and ripple are generated in the presence of a large model parameter mismatch. However, on comparing Fig. 14 (a) and (b) it can be seen that the TFS-PCC and PFS-PCC methods still

REFERENCES

[1] H. Abu-Rub, J. Holtz, J. Rodriguez, and B. Ge, "Medium-voltage multilevel converters—state of the art, challenges, and requirements in industrial applications," *IEEE Trans. Ind. Electron.*, Vol. 57, No. 8, pp.2581-2596, Aug. 2010.

[2] M. Malinowski, K. Gopakumar, J. Rodriguez, and M. A. Perez, "A survey on cascaded multilevel inverters," *IEEE Trans. Ind. Electron.*, Vol. 57, No. 7, pp. 2197-2206, Jul. 2010.

[3] C. Lee, B. Wang, S. Chen, S. Chou, J. Huang, P. Cheng, H. Akagi, and P. Barbosa, "Average power balancing control of a STATCOM based on the cascaded h-bridge PWM converter with star configuration," *IEEE Trans. Ind. Applicat.*, Vol. 50, No. 6, pp.3893-3901, Nov./Dec. 2014.

[4] S. Essakiappan, H. Krishnamoorthy, P. Enjeti, R. Balog, and S. Ahmed, "Multilevel medium-frequency link inverter for utility scale photovoltaic integration," *IEEE Trans. Power Electron.*, Vol. 30, No. 7, pp. 3674-3684, Jul. 2015

[5] L. Maharjan, T. Yamagishi, H. Akagi, and J. Asakura, "Fault-tolerant operation of a battery-energy-storage system based on a multilevel cascade PWM converter with star configuration," *IEEE Trans. Power Electron.*, Vol. 25, No. 9, pp. 2386-2396, Sep. 2010.

[6] A. S.-Ruiz, M. Mazuela, S. Alvarez, G. Abad, and I. Baraia, "Medium voltage–high power converter Topologies comparison procedure, for a 6.6 kV drive application using 4.5 kV IGBT modules," *IEEE Trans. Ind. Electron.*, Vol. 59, No. 3, pp. 1462-1476, Mar. 2012.

[7] J. Chavarria, D. Biel, F. Guinjoan, C. Meza, and J. Negroni, "Energy-balance control of PV cascaded multilevel grid-connected inverters under level-shifted and phase-shifted PWMs," *IEEE Trans. Ind. Electron.*, Vol. 60, No. 1, pp. 98-111, Jan. 2013.

[8] J. Rodriguez and P. Cortes, *Predictive Control of Power Converters and Electrical Drivers*, 1st ed. John Wiley & Sons, Inc., 2012.

[9] J. Rodriguez, M. P. Kazmierkowski, J. R. Espinoza, P. Zanchetta, H. Abu-Rub, H. A. Young, and C. A. Rojas, "State of the art of finite control set model predictive control in power electronics," *IEEE Trans. Ind. Informat.*, Vol. 9, No. 2, pp. 1003-1016, May. 2013.

[10] W. Xie, X. Wang, F. Wang, W.Xu, R. M. Kennel, D. Gerling, and R. D. Lorenz, "Finite-control-set model predictive torque control with a deadbeat solution for pmsm drives," *IEEE Trans. Ind. Electron.*, Vol. 62, No. 9, pp. 5402-5410, Sep. 2015.

[11] S. Kwak, S.-E. Kim, and J.-C.l Park, "Predictive current control methods with reduced current errors and ripples for single-phase voltage source inverters," *IEEE Trans. Ind. Informat.*, Vol. 11, No. 5, pp. 1006-1016, Oct. 2015.

[12] S. Kwak, U.-C. Moon, and J.-C. Park, "Predictive-control-based direct power control with an adaptive parameter identification technique for improved AFE performance," *IEEE Trans. Power Electron.*, Vol. 29, No. 11, pp. 6178-6187, Nov. 2014.

[13] P. Karamanakos, K. Pavlou, and S. Manias, "An enumeration-based model predictive control strategy for the cascaded h-bridge multilevel rectifier," *IEEE Trans. Ind. Electron.*, Vol. 61, No. 7, pp. 3480-3489, Jul. 2014.

[14] R. O. Ramirez, J. R. Espinoza, P. E. Melin, M. E. Reyes, E. E. Espinosa, C. Silva, E. Maurelia, "Predictive controller for a three-phase/single-phase voltage source converter cell," *IEEE Trans. Ind. Informat.*, Vol. 10, No. 3, pp. 1878-1889, Aug. 2014.

[15] A. Fernandez, P. Rodríguez, G. Escobar, C. Pozos, and J. Sosa, "A model-based controller for the cascade h-bridge multilevel converter used as a shunt active filter," *IEEE Trans. Ind. Electron.*, Vol. 60, No. 11, pp. 5019-5028, Nov. 2013.

[16] L. Tarisciotti, P. Zanchetta, A. Watson, S. Bifaretti, and J. C. Clare, "Modulated model predictive control for a seven-level cascaded h-bridge back-to-back converter," *IEEE Trans. Ind. Electron.*, Vol. 61, No. 10, pp. 5375-5384, Oct. 2014.

[17] C. D. Townsend, T. J. Summers, and R. E. Betz, "Multigoal heuristic model predictive control technique applied to a cascaded h-bridge statcom," *IEEE Trans. Power Electron.*, Vol. 27, No. 3, pp. 1191-1200, Mar. 2012.

[18] P. Zanchetta, D. B. Gerry, V. G. Monopoli, J. C. Clare, and P. W. Wheeler, "Predictive current control for multilevel active rectifiers with reduced switching frequency," *IEEE Trans. Ind. Electron.*, Vol. 55, No. 1, pp. 163-172, Jan. 2008

[19] P. Cortes, A. Wilson, S. Kouro, J. Rodriguez, and H. Abu-Rub, "Model predictive control of multilevel cascaded h-bridge inverters," *IEEE Trans. Ind. Electron.*, Vol. 57, No. 8, pp. 2691-2699, Aug. 2010.

[20] C. A. Rojas, S. Kouro, R. Ruiz, S. Rivera, B. Wu, and X. Guo, "Multiobjective predictive control of a three-phase seven-level cascaded h-bridge converter for grid-connected photovoltaic systems," in *Proc. ISIE*, pp. 1121-1126, 2015.

[21] A. Wilson, P. Cortes, S. Kouro, J. Rodriguez and H. Abu-Rub, "Model predictive control for cascaded h-bridge multilevel inverters with even power distribution," *in Proc. ICIT*, pp. 1271-1276, 2010.

[22] S. Kwak, and J.-C. Park, "Switching strategy based on model predictive control of VSI to obtain high efficiency and balanced loss distribution," *IEEE Trans. Power Electron.*, Vol. 29, No. 9, pp. 4551-4567, Sep. 2014.

[23] S. Kwak, and J.-C. Park, "Predictive control method with future zero-sequence voltage to reduce switching losses in three-phase voltage source inverters," *IEEE Trans. Power Electron.*, Vol. 30, No. 3, pp. 1558-1566, Mar. 2015.

[24] S. Kwak, and S.-k. Mun, "Model predictive control methods to reduce common-mode voltage for three-phase voltage source inverters," *IEEE Trans. Power Electron.*, Vol. 30, No. 9, pp.5019-5035, Sep. 2015

[25] H.-T. Moon, H.-S. Kim, and M.-J. Youn, "A discrete-time predictive current control for pmsm," *IEEE Trans. Power Electron.*, Vol. 18, No. 1, pp. 464-472, Jan. 2003.

[26] R. P. Aguilera and D. E. Quevedo, "On stability and performance of finite control set mpc for power converters," in *Proc. PRECEDE*, 2011.

[27] R. P. Aguilera and D. E. Quevedo, "Predictive control of power converters: designs with guaranteed performance," *IEEE Trans. Ind. Informat.*, Vol. 11, No. 1, pp. 53-63, Feb. 2015.

Chen Qi received his B.S. and Ph.D. degrees from the School of Electrical Engineering, Dalian University of Technology, Dalian, China, in 2009 and 2014, respectively. He is presently a Postdoctoral Fellow in the Rolls-Royce@NTU Corporate Lab, Nanyang Technological University, Jurong West, Singapore. His current research interests include multilevel converters, matrix converters, model predictive control, and random modulation.

Pengfei Tu received his B.S. degree from Wuhan University, Wuhan, China, in 2013; and his M.S. degree from the Nanyang Technological University, Jurong West, Singapore, in 2014, where he is presently working towards his Ph.D. degree. His current research interests include the reliability of multilevel converters.

Peng Wang received his B.S. degree from Xian Jiaotong University, Xian, China, in 1978; his M.S. degree from the Taiyuan University of Technology, Taiyuan, China, in 1987; and his M.S. and Ph.D. degrees in Power Engineering from the University of Saskatchewan, Saskatoon, SK, Canada, in 1995 and 1998, respectively. He is presently working as a Full Professor at the Nanyang Technological University, Jurong West, Singapore.

Michael Zagrodnik is presently working as a Project Manager at Rolls-Royce@NTU Corporate Lab, Nanyang Technological University, Jurong West, Singapore. His current research interests include cooling systems, multilevel converters, and marine propulsion.